Applied Catalysis B: Environmental 270 (2020) 118891

Contents lists available at ScienceDirect

Applied Catalysis B: Environmental

journal homepage: www.elsevier.com/locate/apcatb

CNTs/ferrihydrite as a highly efficient heterogeneous Fenton catalyst for the degradation of bisphenol A: The important role of CNTs in accelerating Fe (III)/Fe(II) cycling

Runliang Zhu[a,*], Yanping Zhu[a,b,c], Haiyang Xian[a,b], Lixia Yan[a,b], Haoyang Fu[a,b], Gangqiang Zhu[d,*], Yunfei Xi[c], Jianxi Zhu[a], Hongping He[a]

[a] CAS Key Laboratory of Mineralogy and Metallogeny, Guangdong Provincial Key Laboratory of Mineral Physics and Materials, Guangzhou Institute of Geochemistry, Chinese Academy of Sciences (CAS), Guangzhou, 510640, China
[b] University of Chinese Academy of Sciences, Beijing, 100049, China
[c] School of Earth, Environmental and Biological Sciences, Queensland University of Technology (QUT), Brisbane, Queensland, 4001, Australia
[d] School of Physics and Information Technology, Shaanxi Normal University, Xi'an, 710062, China

ARTICLE INFO

Keywords:
Ferrihydrite
CNTs
Heterogeneous Fenton catalysis
Fe(III)/Fe(II) redox cycling
H_2O_2 decomposition

ABSTRACT

The generation of Fe(II) from Fe(III) is the rate-limiting step in the heterogeneous Fenton reaction, and accelerating this step is critical for enhancing the reaction efficiency and also the subject of extensive studies. In this work, the oxidized multi-walled carbon nanotubes (CNTs) were coupled with ferrihydrite (Fh) to synthesize novel and highly efficient heterogeneous Fenton catalysts (CNTs/Fh). Interestingly, the calculated apparent rate constants by 3%CNTs/Fh could reach ~7.1 times as high as that by Fh, well in agreement with the accelerated decomposition rate of H_2O_2, as well as the enhanced generation rate of Fe(II) and hydroxyl radicals in the CNTs/Fh system. The density functional theory calculations and the cyclic voltammograms curves both well indicated that the Fe(III)/Fe(II) redox cycling on CNTs/Fh could be significantly enhanced during the Fenton reaction, from both dynamic (accelerating the electron transfer from H_2O_2 to Fh) and thermodynamic (lowering Fe(III)/Fe(II) redox potential) aspects.

1. Introduction

In recent years, heterogeneous Fenton reaction has received increasing concerns for wastewater treatment, which has a broader optimal pH range and can avoid the production of a large amount of sludge, as compared with traditional homogeneous Fenton reaction [1–7]. However, the heterogeneous Fenton reaction is still hampered due to the low generation rate of Fe(II) from Fe(III), which is also known as the rate-limiting step (Eq. (1)). A large number of recent studies, therefore, focused on searching for effective and facile strategies to accelerate the reduction of Fe(III) to Fe(II), which then can promote the decomposition of H_2O_2 into hydroxyl radicals ($HO^{\cdot}$) (Eq. (2)) [8–11].

$$\equiv Fe(III) + H_2O_2 \rightarrow \equiv Fe(II) + HO_2^{\cdot} + H^+ \quad (1)$$

$$\equiv Fe(II) + H_2O_2 \rightarrow \equiv Fe(III) + HO^{\cdot} + OH^- \quad (2)$$

One of these strategies is to combine electron-rich donors, such as nano zero-valent iron (nZVI) [10,12,13], carboxylic acids (e.g., EDTA, oxalate, and citrate) [14–16], and other reducing species (e.g., hydroxylamine) [3,17], with the heterogeneous Fenton catalysts, and the transferred electrons from these donors can accelerate the generation of Fe(II) and then promote the decomposition of H_2O_2, resulting in high heterogeneous Fenton reactivity. However, multiple recycling of these species is hard to achieve, as the available electrons from the donor component on these materials are limited. Besides, the accumulation of ferric oxyhydroxides on the surface of nZVI in neutral to slightly alkaline environments will reduce the reactive surface area for the formation of hydroxyl radicals and hamper the electron supply from nZVI [18]. Recently, several studies introduced photo-generated electrons from semiconductors and plasmonic catalysts (e.g., $BiVO_4$, TiO_2, Ag/AgX (X=Cl, Br)) to accelerate the regeneration of Fe(III) [8,9,19–21]. This strategy can continuously inject photo-generated electrons to heterogeneous Fenton catalysts for the reduction of Fe(III), and the photo-generated holes can also contribute to the degradation of organic contaminants [20]. Nevertheless, this strategy depends on continuous light irradiation, which will hamper its application in the areas that can

* Corresponding authors.
E-mail addresses: zhurl@gig.ac.cn (R. Zhu), zgq2006@snnu.edu.cn (G. Zhu).

https://doi.org/10.1016/j.apcatb.2020.118891
Received 19 December 2019; Received in revised form 8 March 2020; Accepted 14 March 2020
Available online 18 March 2020

hardly introduce light irradiation during the reaction processes, such as groundwater treatment.

Carbon-based nanomaterials, such as carbon nanotubes [21–23], polyhydroxy fullerenes [24], graphene oxide [7,25], activated carbon [26,27], biochar [28,29], and hydrothermal carbon [30], together with their functionalized products, have also been widely applied in heterogeneous Fenton reactions by combining with iron ions, due to their abundant electrons, large specific surface areas (SSA), and ubiquitous existence in natural environments. Among them, oxidized multi-walled carbon nanotubes (CNTs), with negatively-charged groups (e.g., carboxyl, hydroxyl, and ether) on their surfaces, have shown great potential to enhance the heterogeneous Fenton reactivity [21,22]. The important roles of CNTs in these reactions have aroused wide discussions but still remain controversial. Several studies deduced that, in a heterogeneous Fenton-like reaction, CNTs could be regarded as an electron-transfer catalyst, just like the Haber–Weiss mechanism involving the reduced and oxidized catalyst states (Eqs. (3) and (4)) [31]. Seo et al. claimed that the enhanced decomposition of H_2O_2 to $HO^{\cdot}$ resulted from the reductive generation of Fe(II) by CNTs (Eq. (5)) [32]; while Peng et al. found that in the absence of H_2O_2, the generation of Fe (II) from Fe(III) did not show any change with increasing MWCNTs−COOH contents [33]. In addition, Yang et al. proposed that 80 % of Fe(II) was formed via a fast reduction of CNT-Fe(III) complexes by H_2O_2 rather than by CNTs [22]. In this term, although these studies all verified that CNTs presented a significant boost in the heterogeneous Fenton reactions, the essential roles of CNTs have not been clarified yet, which still need in-depth study.

$$CNTs + H_2O_2 \rightarrow CNTs^+ + HO^{\cdot} + OH^- \quad (3)$$

$$CNTs^+ + H_2O_2 \rightarrow CNTs + HO_2^{\cdot} + H^+ \quad (4)$$

$$CNTs + Fe(III) \rightarrow CNTs^+ + Fe(II) \quad (5)$$

Theoretically, beside the direct injection of external electrons (e.g., from electron-rich materials and photo-generated electrons) to catalysts, promoting the electron transferring speed between catalysts and H_2O_2, and decreasing the redox potential of Fe(III)/Fe(II) can also effectively facilitate the redox cycling of Fe(III)/Fe(II). One would, therefore, wonder whether the redox potential of Fe(III)/Fe(II) can be lowered (from the thermodynamic perspective) to enhance the Fenton reactivity in the CNT-Fe(III) system. Indeed, a number of studies showed that chelating agents (e.g., oxalate and EDTA) with rich carboxyl groups could be combined with iron ions, which then would decrease the redox potential of Fe^{3+}/Fe^{2+} [15,34]. For example, the redox potential of Fe^{3+}/Fe^{2+} was 0.77 V (vs. NHE), but it decreased to 0.356, 0.256, and 0.209 V (vs. NHE) after being combined with disodium nitrilotriacetate, oxalate, and EDTA, respectively [34]. This property could help to accelerate the reduction of Fe(III) by H_2O_2 and subsequently enhance the Fenton catalytic activity. Being enlightened by these studies, we propose that combining CNTs (with oxygen-rich functional groups) and heterogeneous Fenton catalysts can not only accelerate the redox cycling of Fe(III)/Fe(II) but also possibly decrease the redox potential of Fe(III)/Fe(II) as well, promoting the decomposition of H_2O_2 from both dynamic and thermodynamic aspects. This hypothesis is the main objective of this study.

Another reason motivates this study is that both iron (oxyhydr) oxide mineral nanoparticles and carbon nanomaterials (from both natural and anthropogenic sources) are ubiquitous in soil, and thus they have a large chance to form nanocomposites [35]. In this term, these nanocomposites, by acting as heterogeneous Fenton catalysts, may play important role in degrading organic contaminants during the soil remediation process using H_2O_2 as oxidant, and it is of high necessity to examine their heterogeneous Fenton reactivity. Among the various iron (oxyhydr)oxide minerals, Fh is a typical iron nanomineral with a rather small particle size (2 − 6 nm) and large SSA (~300 m^2/g) [5,36]. Fh widely exists in soil and has been served as a highly efficient heterogeneous Fenton catalyst [4,5,37]. Besides, the small particle size and positively charged surface of Fh make it facile in coupling with the negatively charged carbon nanomaterials.

In this work, we combined Fh with oxidized multi-walled CNTs, with the purpose of (1) synthesizing novel and highly efficient heterogeneous Fenton catalysts (i.e., CNTs/Fh) and (2) clarifying the important roles of CNTs in the Fenton reactions of CNTs/Fh. The structural characteristics and the heterogeneous Fenton catalytic activity of the as-synthesized catalysts were studied. The concentrations of Fe(II), the decomposition rate of H_2O_2, the production rate of $HO^{\cdot}$, and the catalytic reactivity of catalysts in the heterogeneous Fenton reaction process were measured. In addition, the density functional theory (DFT) calculations for CNTs/Fh were conducted to analyze the specific role of CNTs in the heterogeneous Fenton system. The cyclic voltammograms (CV) were measured to investigate the redox processes of Fh and CNTs/Fh. These results indicated that the introduction of CNTs can facilitate the decomposition of H_2O_2 to $HO^{\cdot}$ by accelerating the redox cycling of Fe(III)/Fe(II) and lowering the redox potential of Fe(III)/Fe(II), resulting in the significant enhancement of the heterogeneous Fenton reactivity for CNTs/Fh.

2. Materials and methods

2.1. Materials

$Fe(NO_3)_3{\cdot}9H_2O$, NaOH, HCl, HNO_3, Na_2CO_3, NH_4F, CH_3COONH_4, CH_3COOH, o-phenanthroline (o-phen), H_2O_2 (30 wt. %), *p*-benzoquinone (BQ), and isopropanol (IPA) were purchased from Shanghai Chemical Reagent Corporation, China. Benzoic acid (BA), *p*-hydroxybenzoic acid (*p*-HBA) (99 %), trifluoroacetic acid (TFA), and acetonitrile were obtained from Aladdin Industrial Corporation (Shanghai, China). 2,9-dimethyl-1,10-phenanthroline (DMP), KH_2PO_4, and $CuSO_4{\cdot}5H_2O$ were purchased from Sigma-Aldrich. BPA was purchased from Macklin Reagent Company. K_2HPO_4 was obtained from Ajax Finechem. The raw CNTs were purchased from Chengdu Organic Chemistry Company Co. Ltd, China. All reagents were used as received.

2.2. Synthesis of Fh, oxidized CNTs, and CNTs/Fh

Two-line Fh was synthesized according to the method described by Xu et al. [4]. In brief, NaOH solution (6 M) was slowly titrated into the $Fe(NO_3)_3{\cdot}9H_2O$ solution (1 M, 40 mL) under vigorous stirring until the final pH was stabilized at 7 ± 0.1. After that, the mixture solution was aged under vigorous stirring for 3 h and then was centrifuged and washed several times using ultra-pure water and ethanol. After being freeze-dried, these samples were ground to pass through a 200-mesh sieve.

The raw CNTs were heated in 30 % HNO_3 at 130 °C for 24 h equipped with a water-cooled reflux condenser. The suspension was washed with ultra-pure water until the pH reached 7.0. After that, the products were separated from the mother liquor by suction filtration. The material was dried overnight at 80 °C in a thermostated oven. After that, the resulting material was crushed to powder and ground to pass through a 200-mesh sieve.

To prepare CNTs/Fh, an appropriate amount of oxidized CNTs (0.01, 0.03, 0.05, or 0.1 g) and Fh powder (1 g) were added into 100 mL ultra-pure water. The mixture was sonicated for 30 min and stirred for 9 h. The precipitates were centrifuged and washed using ultra-pure water and ethanol. After being freeze-dried, the materials were ground to pass through a 200-mesh sieve. According to the calculated weight ratio of CNTs to Fh, the resulting materials were labeled as 1%CNTs/Fh, 3%CNTs/Fh, 5%CNTs/Fh, and 10%CNTs/Fh.

2.3. Characterization

XRD patterns were obtained using a Bruker D8 ADVANCE X-ray

diffractometer (Karlsruhe, Germany) with Cu Kα radiation, operating at 40 mA and 40 kV. The patterns were collected over the 2θ range of 3–80° at a scanning speed of 3°/min. The scanning electron microscopy (SEM) images were recorded by a field emission scanning electron microscopy (Carl Zeiss SUPRA55SAPPHIR). Transmission electron microscopy (TEM) images were obtained using FEI Talos F200S instrument at an acceleration voltage of 200 kV with energy dispersive X-ray spectroscopy (EDS) (Super X) for the determination of metal composition. X-ray photoelectron spectroscopy (XPS) analyses were carried out by a Thermo Fisher Scientific K-Alpha spectrometer. The C1 s peak from the adventitious carbon-based contaminant with bind energy of 284.80 eV was used as the reference for calibration. Nitrogen adsorption-desorption isotherms were determined on a Micromeritics ASAP 2020 M instrument. All of the samples were degassed for 12 h at 60 °C prior to N_2 adsorption measurements. The SSA value of these samples was calculated from the obtained N_2 adsorption data using the multi-point Brunauer–Emmett–Teller (BET) equation. Zeta potential measurements of samples were carried out by a Zetasizer Nano ZS90 instrument. All data were determined 3 times in each pH, and the average value was plotted to analyze the isoelectric point of the sample. CV measurements were performed at 10 mV s^{-1} for each sample. All experiments were performed at ambient temperature (22 ± 2 °C) and pH 3, and the electrode potentials were converted to the RHE scale by E (RHE) = E (SCE) + 0.244 V + 0.059 × pH.

2.4. DFT calculations details

At the DFT level, all of the calculations were performed using the Vienna Ab initio Simulation Package (VASP) [38] with the pseudopotential of projector augmented wave (PAW) [39]. The cutoff energy was set to 650 eV [40] for a 10^{-5} convergence of the total energy. PBE + U with a *U-J* parameter of 3.0 eV [41] was employed to deal with Fe 3d electrons. We employed a cluster model of Fh with unit cell-size ($Fe_{10}O_{35}H_{22}$) according to the model from Michel et al. [42]. The multi-walled CNTs were simplified by single-walled CNTs, which was modeled by one layer of hexagon units with 48 C atoms. A COOH group was added at the rim of CNTs for the representation of functionalized groups. For both Fh and functionalized CNTs, extra H atoms were added to saturate the dangling bonds of the cluster models. The CNTs/Fh composite was modeled through a dehydration reaction between CNTs and Fh via the COOH group, which forms a Fe—O—C bond connecting both the clusters. All of the clusters were modeled in a 30 × 30 × 30 $Å^3$ box.

2.5. Heterogeneous Fenton catalytic experiments

The heterogeneous Fenton degradation of BPA by these catalysts was conducted in a 100 mL conical flask. The initial pH value of the solution (pH = 3) was adjusted by adding 0.1 M NaOH and HNO_3. 50 mg catalyst and 50 mL BPA (30 mg/L) solution were added into the above conical flask under vigorously stirring for 30 min to reach the adsorption-desorption equilibrium between the catalysts and BPA as the BPA adsorption on as-prepared catalysts can reach equilibrium within 30 min (Fig. S1). After that, 0.5 mL 1 M H_2O_2 was dropped into the above solution. At given time intervals, the suspension was collected and filtered immediately with 0.22 μm membrane filters.

The concentration of the BPA was analyzed using an Agilent 1260 HPLC equipped with a UV absorbance detector. A Luna 5μ C18 column (250 mm) was used for the HPLC separation. A 20 μL sample was injected into the HPLC system for analysis with a flow rate of 0.8 mL/min at room temperature. The mobile phase consisted of acetonitrile and water (50:50, v/v) and the analysis wavelength was selected as 230 nm [43]. The total organic carbon (TOC) was measured using a Shimadzu TOC-V total organic carbon analyzer. The total Fe ionsleaching was determined by atomic absorption spectrophotometry (AAS, PerkinElmer AAnalyst 400, America). The concentration of H_2O_2 was calculated by a spectrophotometric method using Copper(II) ion and DMP [44]. 1 g DMP reagent was dissolved in 100 mL of ethanol and was stored in a brown bottle at 4 °C. A phosphate buffer solution (0.1 M) was prepared from K_2HPO_4 and KH_2PO_4 with pH adjusted to 7.0. After that, 0.5 mL of the reaction solution, DMP, $CuSO_4{\cdot}5H_2O$ (0.01 M), and phosphate buffer were added to a 50 mL volumetric flask to form a bright yellow complex ($Cu(DMP)^{2+}$). The concentration of $Cu(DMP)^{2+}$ was measured via UV–vis spectroscopy (759S, Shanghai JingHua Instrument Co. Ltd., China) at 454 nm.

The concentration of Fe(II) on the surface of the as-prepared samples was measured according to the method of Xu et al. [4] with some modifications, which is similar to a common method for the measurement of Fe(II) in the iron ore. At a given time interval, 1 mL 6 M HCl, 0.2 g Na_2CO_3, and 2 mL 10 M NH_4F were added into the precipitation after centrifugation to dissolve Fh entirely and prevent Fe(II) from being oxidized to Fe(III). After that, 1 mL CH_3COONH_4—CH_3COOH buffer solution (pH 4.2) and 1 mL 0.5 % (m/v) o-phen were added into above solution to form an orange complex in acidic solution. The concentration of complex was measured via UV–vis spectroscopy with maximum absorption at 510 nm.

2.6. Analysis of reactive species

Free radical capture experiments were conducted to ascertain the reactive species in the heterogeneous Fenton degradation of BPA. IPA and BQ were chosen as scavenges of $HO^{\cdot}$ and superoxide radical ($O_2^{\cdot-}$), respectively. The experimental details for free radicals capture processes were similar to the heterogeneous Fenton catalytic experiment. The oxidation of BA (10 mM) to *p*-HBA at an initial pH value of 3 was used as a probe reaction for quantifying the production of $HO^{\cdot}$ in the process of heterogeneous Fenton catalysis [45]. *p*-HBA was also quantitatively analyzed using the Agilent 1260 HPLC equipped with a Luna 5μ C18 column (250 mm). The mobile phase was a mixture of 0.1 % TFA aqueous solution and acetonitrile (65:35, v/v) at a flow rate of 1 mL/min, with the detection wavelength at 255 nm [45,46].

3. Results and discussion

3.1. Structural characterization results

The XRD patterns of raw multi-walled CNTs and oxidized multi-walled CNTs (CNTs) are similar and display two distinct reflections at 26.0° and 43.8° (Fig. S2), which correspond to the (002) and (100) diffraction planes of CNTs, respectively [47]. As shown in Fig. 1a, Fh shows two broad reflections at 35.1° and 63.3°, well consistent with previous reports for 2-line Fh [8]. After combining CNTs with Fh, the XRD patterns have no obvious changes except for the appearance of the characteristic reflection of CNTs.

The SSA of pure Fh and CNTs are 273 and 139 m^2/g, respectively (Table S1). After introducing CNTs, the SSA of the composites increases at first and then decreases as the CNTs content exceeds 3 %. Specifically, the SSA of 3%CNTs /Fh can even reach 387 m^2/g. The significant increase of SSA may be ascribed to the strong interaction between CNTs and Fh, and the Fh nanoparticles can well disperse on CNTs, creating more micro- and mesopores. This hypothesis will be further supported by SEM and TEM characterizations later.

The Zeta potential values of CNTs, Fh, and 3%CNTs/Fh were also collected to verify the strong interactions between CNTs and Fh (Fig. 1b). CNTs exhibit negative charge at the pH range of 2.0–9.0 while the zeta potential of Fh is about 6.5. Therefore, CNTs and Fh should have strong electrostatic interaction under pH 6.5. The charge value of 3%CNTs/Fh is a little bit lower than that of pure Fh after combing with CNTs, consistent with the previous study. The decreased charge value of 3%CNTs/Fh may be due to the formation of Fe—O—C bonds between CNTs and Fh, which will be verified below. In addition, Xu et al. synthesized fullerol modification Fh, and they also demonstrated the

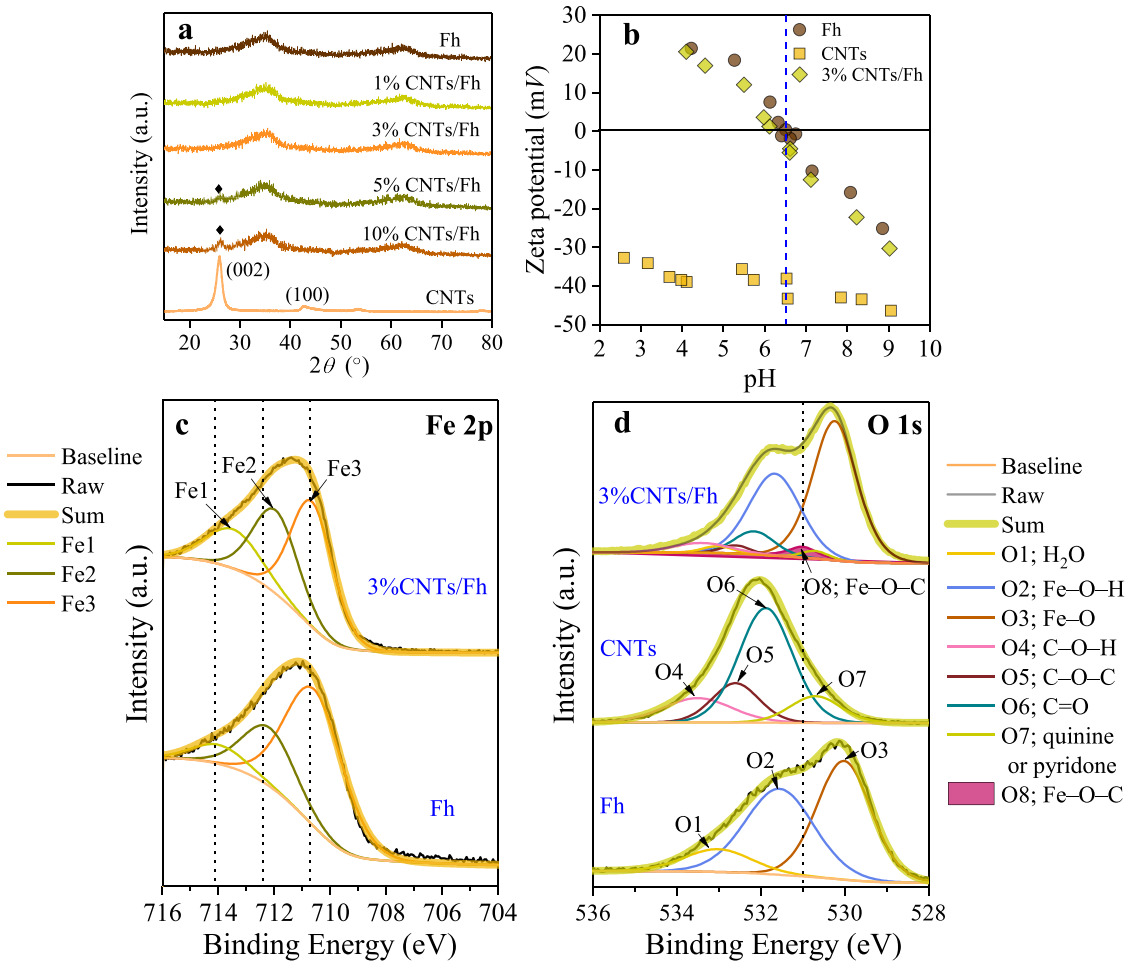

Fig. 1. (a) XRD patterns and (b) Zeta potential of the as-prepared catalysts; (c) Fe $2p_{3/2}$ XPS spectra of Fh and 3%CNTs/Fh; (d) O 1s XPS spectra of Fh, CNTs, and 3%CNTs/Fh.

formation of covalent bonds between the hydroxyl groups on fullerol and Fh [24]. Thus, we speculated that the surface complexes may also form between the oxygen-containing functional groups of CNTs and the surface hydroxyl groups on Fh, which will be further verified below. With these strong interactions between CNTs and Fh, we believe Fh nanoparticles can well disperse on CNTs.

The SEM image of raw CNTs shows the integrated tubular structures of CNTs with a diameter of 20–40 nm and length of 200–500 nm (Fig. S3). After being treated with HNO_3, the length of the nanotubes decreases, and the surfaces of the nanotubes are also eroded, indicating that CNTs were oxidized by HNO_3. Fig. 2a shows that pure Fh presents the aggregations of nanoparticles. CNTs also show large accumulation with nano-scale tubes. After combining CNTs with Fh, the particles become fluffier, and these two materials both distribute uniformly, due to their strong interactions. In addition, the SEM images of 3%CNTs/Fh show that Fh nanoparticles with different size wrap around CNTs, and some small particles with a size of 5–10 nm can be observed on the tubes, indicating a good dispersity of Fh on CNTs, which may be due to the formation of Fe—O—C bonds between CNTs and Fh, well consistent with the result of Zeta potential.

To identify the formation of Fe—O—C bonds between Fh and CNTs, the Fe $2p_{3/2}$ XPS spectra of Fh and 3%CNTs /Fh were compared, as shown in Fig. 1c. Three peaks located at 710.67 (Fe1), 712.18 (Fe2), and 713.98 eV (Fe3) are attributed to the binding energies of Fe(III)—O on Fh [5,48]. After combing Fh with CNTs, the peaks of Fe2 and Fe3 were shifted to 711.95 and 713.47 eV, respectively, in the Fe $2p_{3/2}$ XPS spectrum of 3%CNTs /Fh. The shift of these peaks may be due to the acquirement of electrons from CNTs, suggesting the formation of Fe—O—C bonds between Fh and CNTs, well consistent with the previous study [49]. In addition, three peaks located at 530.10, 531.55, and 533.02 eV were observed in the O 1s XPS spectrum of Fh, which were assigned to Fe—O (O1), Fe—OH (O2), and adsorbed water (O3), respectively (Fig. 1d). The O1s XPS spectrum of CNTs can be divided into four peaks: C—O—H (O4; 533.40 eV); C—O—C (O5; 532.60 eV); C═O (O6; 531.88 eV); the highly conjugated forms of carbonyl oxygen such as quinine or pyridone groups (O7; 530.70 eV) [50,51]. After combing CNTs with Fh, a new peaks located at 531.10 eV appears in the O1s XPS spectrum of 3%CNTs/Fh, which should belong to the Fe—O—C bonds formed between Fh and CNTs, well consistent with other carbon-iron oxide composites reported by previous studies [52,53].

The microstructural and morphological details of 3%CNTs/Fh were further obtained by TEM and HRTEM (Fig. 2b). The obtained results clearly showed that Fh nanoparticles well attached to the surface of CNTs. The interplanar spacing of 0.35 nm is attributed to the (002) basal planes in the carbon layer, well consistent with the XRD results and other studies [21,54]. The elemental mapping further reveals that Fe, O, and C elements are uniformly distributed throughout the composites. As such, both the SEM and TEM results well showed the relatively uniform structure of CNTs/Fh composites, which should result from the strong interactions between CNTs and Fh, and also resulted in large SSA values.

3.2. Degradation of BPA

The heterogeneous Fenton catalytic activities of CNTs/Fh samples were studied by choosing BPA as the target contaminant (Fig. 3a). Only

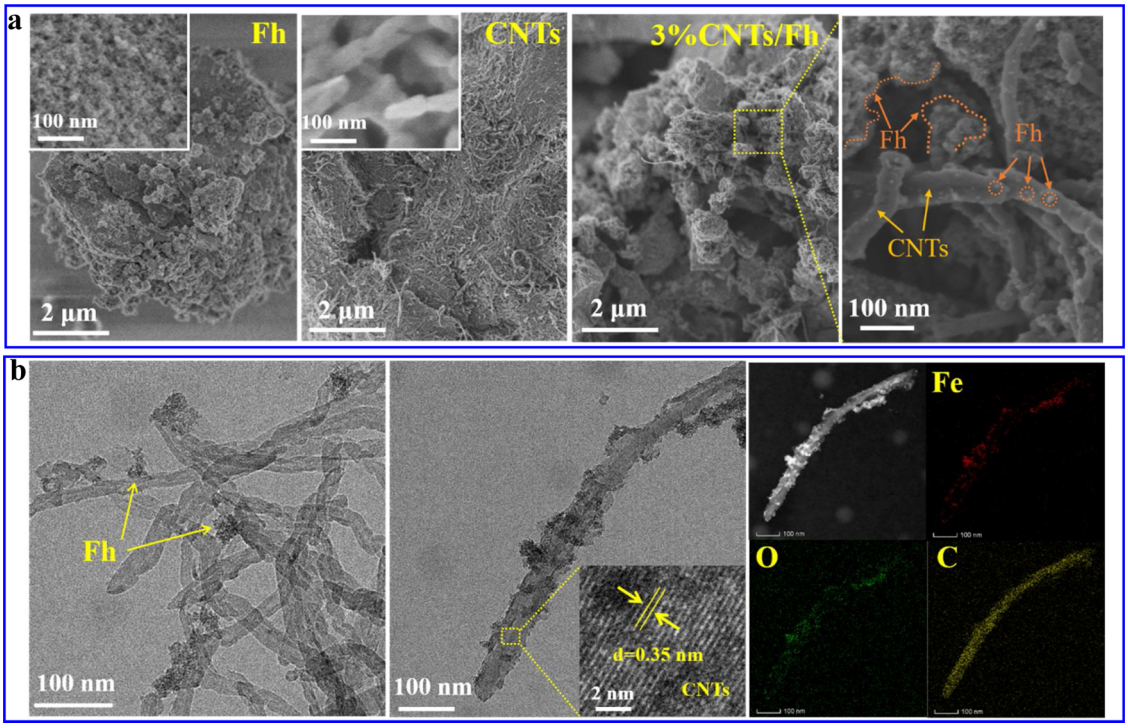

Fig. 2. (a) SEM images of the as-prepared catalysts; (b) TEM and HRTEM images of 3%CNTs/Fh.

about 4.57 % BPA can be degraded by pure H_2O_2, indicating that the oxidation capacity of H_2O_2 is insufficient to degrade BPA. Nearly 37 % of BPA can be adsorbed by pure CNTs within 30 min, well consistent with the excellent adsorption property of CNTs reported in previous studies [55,56]. Both Fh and CNTs/Fh show much weaker adsorption capacity toward BPA than CNTs. After adding H_2O_2, rather a weak removal of BPA can be achieved by pure CNTs, which suggests that CNTs alone can hardly decompose H_2O_2 to produce HO˙. As for pure Fh, nearly 36 % BPA can be removed with the addition of H_2O_2. After combing with CNTs, the removal efficiency of BPA by CNTs/Fh increases dramatically. Specifically, the degradation efficiency of BPA first increases with rising CNTs content (from 0 to 3 %) and then begins

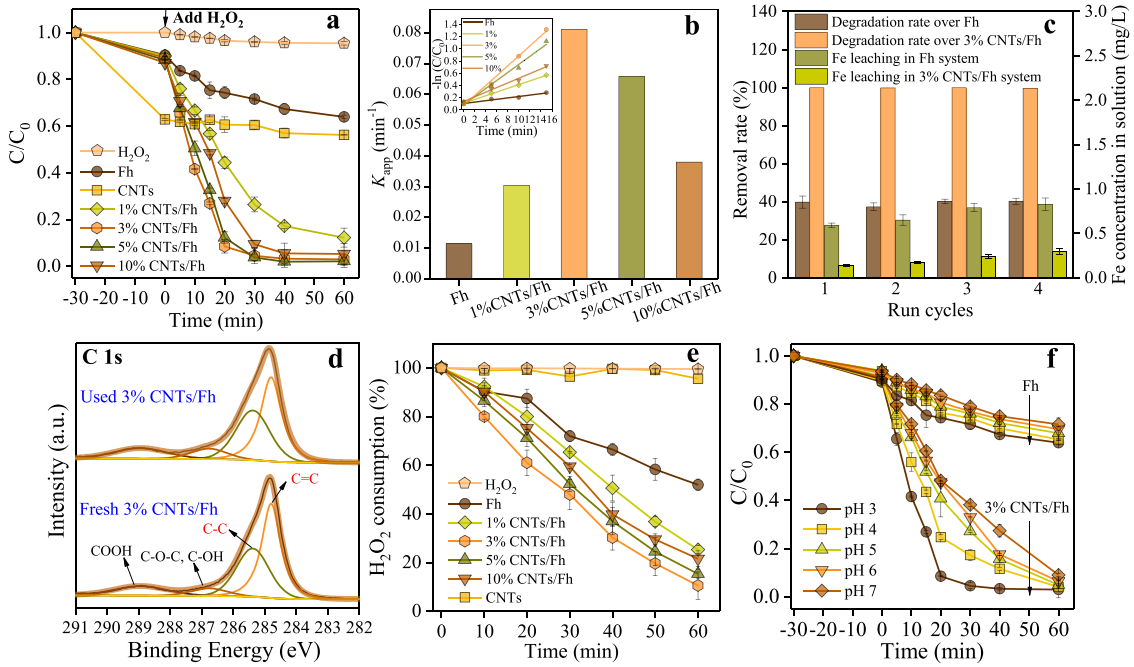

Fig. 3. (a) Degradation kinetics; (b) apparent degradation rate constants; (c) stability tests for the degradation of BPA by as-prepared catalysts; (d) C1s XPS spectra of 3%CNTs/Fh before and after the degradation of BPA within 60 min; (e) H2O2 consumption in the heterogeneous Fenton reaction over as-prepared catalysts; (f) effect of different initial pH on the degradation of BPA by Fh and 3%CNTs/Fh. Inset of (b): pseudo-first-order kinetics for the degradation of BPA on these samples (the pseudo-first-order kinetics on CNTs is absent due to the rather low BPA degradation rate).

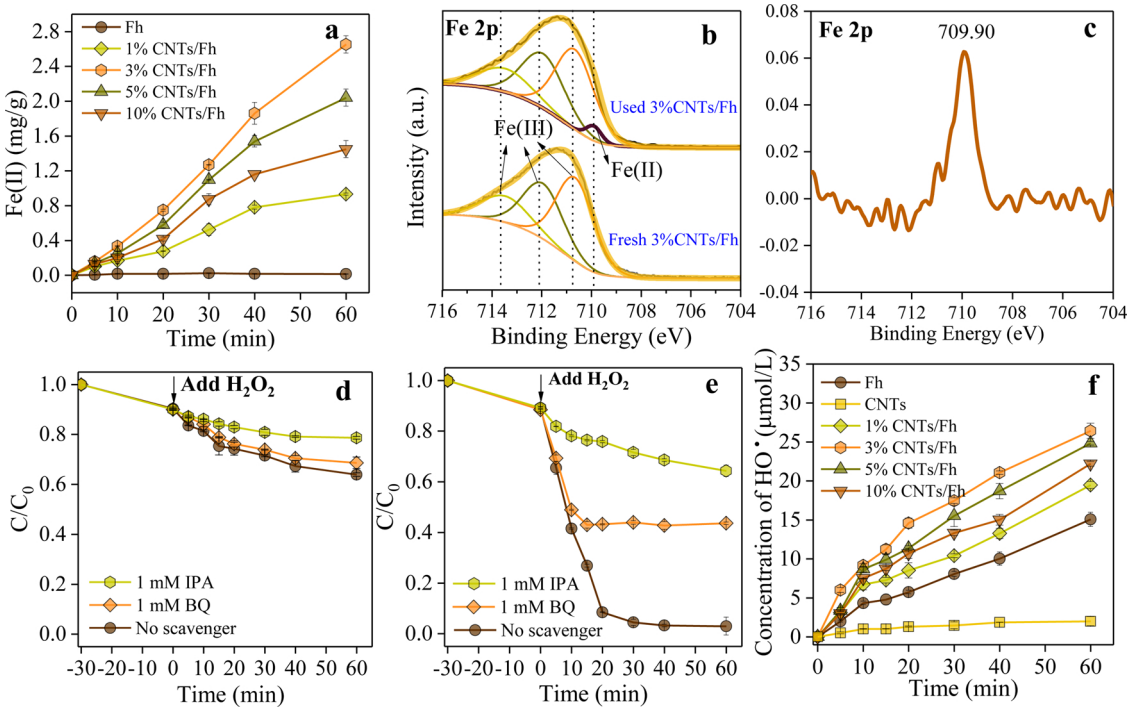

Fig. 4. (a) Concentration of Fe(II) on catalysts in the heterogeneous Fenton reaction process; (b) Fe $2p_{3/2}$ XPS spectra of fresh 3%CNTs/Fh and used 3%CNTs/Fh (reaction for 60 min); (c) Fe $2p_{3/2}$ XPS after subtraction from used 3%CNTs/Fh to fresh 3%CNTs/Fh; degradation of BPA on (d) Fh and (e) 3%CNTs/Fh with the addition of different scavengers; (f) concentration of $HO^{\cdot}$ in the heterogeneous Fenton reaction.

to decrease with further rising CNTs content (> 3%). The decrease of SSA (298.4 m^2/g for 5 % CNTs/Fh and 295.4 m^2/g for 10%CNTs/Fh) and the lower Fh contents might be the causes for their decreased catalytic efficiency. Among all of the tested catalysts, 3%CNTs/Fh exhibits the best catalytic activity, with a BPA degradation rate of 96 % within 30 min.

To better compare the heterogeneous Fenton catalytic activities of these samples, the degradation kinetics of BPA over these samples were fitted with the pseudo-first-order equation. The apparent rate constants (K_{app}) were determined from the regression curves of $-\ln(C/C_0)$ versus reaction time (Fig. 3b). Accordingly, the calculated K_{app} of 3%CNTs/Fh is 0.0811 min^{-1}, nearly 7.1 times as high as that of pure Fh (0.0114 min^{-1}). This result further proves that coupling CNTs with Fh can significantly increase the heterogeneous Fenton catalytic activity towards BPA. The TOC removal efficiency of BPA was further examined in this work, and the results further prove that CNTs/Fh has much higher efficiency than Fh in the mineralization of BPA (Fig. S4). Noticeably, the TOC removal rate of BPA by 3%CNTs/Fh can reach 79.1 %, much higher than that by pure Fh (26.7 %).

The repeatability experiments of BPA degradation by Fh and 3%CNTs/Fh were conducted as well (Fig. 3c), and the results show that the degradation of BPA by 3%CNTs/Fh can retain 99.6 % after 4 cycles, which is much higher than those by pure Fh (42.2 %). In addition, the Fe leaching in 3%CNTs/Fh is much lower than that in the Fh system, with a Fe^{3+} concentration of 0.826 and 0.292 mg/L after 4 cycles, respectively, indicating the good stability of CNTs/Fh composites. Zubir et al. demonstrated that in the GO−Fe_3O_4 Fenton-like system, GO plays a sacrificial role via the oxidation of C=C carbon domains, and then transfer their unpaired π electrons to Fe_3O_4 to accelerate the Fe(III)/Fe(II) redox cycles, resulting in the partial consumption of GO during the reaction [7]. In this term, these reactions may not cycle continuously due to the limited unpaired π electrons on carbon materials. Ma et al. proposed that in the CNTs/FeS Fenton-like system, CNTs could reduce Fe(III) to Fe(II) due to their unpaired π electrons and CNTs can be oxidized to $CNTs^+$ at the same time (Eq. (5)) [31]. Moreover, they deduced that CNTs could be regarded as an electron-transfer catalyst, just like the Haber–Weiss mechanism involving the reduced and oxidized catalyst states (Eqs. (3) and (4)), i.e., $CNTs^+$ may react with H_2O_2 to regenerate CNTs (Eq. (4)). As our results showed that CNTs/Fh retained high reactivity in the repeatability experiments, we also propose that CNTs should not be the major electron donor during the Fenton reaction process, and the reduction of Fe(III) should be achieved mainly via accepting electrons from H_2O_2.

To further verify the above hypothesis, the C1s XPS spectra of 3%CNTs/Fh before and after the degradation of BPA (after 4 cycles) were compared (Fig. 3d). The binding energies at 284.8 and 285.4 eV correspond to the sp^2-hybridized graphite-like carbon atoms (C=C) and C−C species in an sp^3 hybridization state [7]. The binding energy at 286.6 eV is attributed to the C−O−H and C−O−C while that at 288.9 eV corresponds to −COOH [57], indicating the presence of several types of functional groups on the oxidized CNTs. After the degradation of BPA, the relative contents belonging to the binding energies of C=C slightly decreased from 47.1 %–44.0 % (Table S2), indicating that little CNTs were oxidized during the degradation of BPA. In addition, the theoretically available electrons of CNTs in the 3%CNTs/Fh composites were roughly calculated (as shown below Table S2), which indicated that the contribution of the electrons from CNTs to the direct reduction of Fe(III) is negligible during the degradation of BPA. Therefore, we can deduce that in the heterogeneous Fenton reaction process, H_2O_2 should be the main electron donors for reducing Fe(III) to Fe(II), while CNTs can accelerate the electron transfer between H_2O_2 and Fh.

The decomposition of H_2O_2 in different systems was determined during the heterogeneous Fenton reaction (Fig. 3e). The results show that H_2O_2 can be hardly decomposed without catalyst and the decomposition of H_2O_2 by pure CNTs is not obvious. Some studies demonstrated that CNTs have the ability to activate H_2O_2 and produce $HO^{\cdot}$ [31]; while several other studies also showed that CNTs had a rather weak ability in activating H_2O_2. Possibly the different oxidized states of CNTs will affect its capacity in activating H_2O_2 [58]. The

decomposition rate of H_2O_2 by pure Fh was 52.8 % within 60 min, in agreement with previous studies showing that Fh can be directly used as heterogeneous Fenton catalysts. After combining CNTs with Fh, the decomposition of H_2O_2 was accelerated significantly, and the optimal CNTs content is 3 %. With nearly 87.5 % H_2O_2 being decomposed by 3%CNTs/Fh within 60 min. The enhancement of the H_2O_2 decomposition rate further verifies that CNTs can promote the electron transfer from H_2O_2 to Fh for the generation of Fe(II), and the presence of high contents of Fe(II) in the CNTs/Fh can well support this hypothesis (Fig. 4).

The effect of initial pH on the heterogeneous Fenton catalytic activity of 3%CNTs/Fh was studied within a wide pH range of 3–7 (Fig. 3f). The catalytic activity of the 3%CNTs/Fh decreases slightly with rising solution pH, but the degradation rate can reach 91.1 % even at neutral pH within 60 min. In comparison, 3%CNTs/Fh exhibits much higher Fenton reactivity at neutral pH (pH = 7; K_{app} = 0.0266 min^{-1}) than Fh at acid condition (pH = 3; K_{app} = 0.0114 min^{-1}) (Fig. S5). These results indicate that 3%CNTs/Fh can efficiently degrade contaminants over a wide pH range, which makes CNTs/Fh a promising candidate for the heterogeneous Fenton reaction.

3.3. Generation of Fe(II) during the heterogeneous Fenton reaction

As proposed above, the introduction of CNTs may accelerate the decomposition of H_2O_2, thus promoting the reduction of Fe(III) to Fe (II). Therefore, the concentration of Fe(II) on these catalysts during the heterogeneous Fenton reaction process was measured (Fig. 4a). Fe(II) can be hardly detected on pure Fh, indicating that the reduction of Fe (III) in the pure Fh system is rather weak. By contrast, Fe(II) content on CNTs/Fh increases dramatically during the whole reaction process, indicating that the introduction of CNTs can accelerate the reduction of Fe(III) to Fe(II), well consistent with the enhanced BPA degradation rate and H_2O_2 decomposition rate. Specifically, the Fe(II) content on 3%CNTs/Fh is the highest, which can even reach 2.6 mg/g within 60 min.

To further verify the existence of Fe(II) on the composites, the Fe $2p_{3/2}$ XPS spectra of 3%CNTs/Fh before and after the degradation of BPA for 60 min were compared (Fig. 4b). No signals of Fe(II) can be observed in the XPS spectrum of fresh 3%CNTs/Fh; however, a signal of Fe(II) appears in the XPS spectrum of 3%CNTs/Fh at 709.9 eV, well consistent with other studies [4,5]. Furthermore, the Fe $2p_{3/2}$ XPS spectra of fresh and used 3%CNTs/Fh were normalized and then the fresh 3%CNTs/Fh was subtracted from the used 3%CNTs/Fh to the obtain the differential spectrum. Fig. 4c presents the obvious binding energy of Fe(II) located at 709.9 eV, which demonstrated that CNTs can promote the reduction of Fe(III) to Fe(II) in the 3%CNTs/Fh system. Zubir et al. suggested that in the heterogeneous Fenton reaction using GO/Fe_3O_4 catalyst, Fe(II) can be regenerated in Fe_3O_4 due to the accelerated electron transfer by the Fe—O—C bonds conjugated in GO/Fe_3O_4 [7]. Similarly, we propose that the chelating effect between CNTs and Fh may also produce Fe—O—C bonds, promoting the decomposition of H_2O_2 and the generation of Fe(II), which will be further verified below using DFT calculation.

3.4. Analysis of the reactive species

As discussed before, $HO^{\cdot}$ and $O_2^{\cdot-}$ could be generated in the heterogeneous Fenton reaction process. Therefore, IPA ($HO^{\cdot}$ scavenger) and BQ ($O_2^{\cdot-}$ scavenger) were added to verify the existence of these two radicals during the heterogeneous Fenton degradation of BPA by Fh and 3%CNTs/Fh. In the pure Fh system (Fig. 4d), the heterogeneous Fenton catalytic activity of BPA is slightly inhibited in the presence of BQ, while a more obvious decrease in the degradation rate can be observed in the presence of IPA. As for the 3%CNTs/Fh system (Fig. 4e), the suppression effects are quite obvious both in the presence of BQ and IPA, with only 56.4 % and 35.7 % BPA being degraded, respectively. These results demonstrated that both $HO^{\cdot}$ and $O_2^{\cdot-}$ contribute to the heterogeneous Fenton degradation of BPA, while $HO^{\cdot}$ plays a more important role in the whole reaction, in agreement with a typical Fenton reaction process. Xu et al. detected that, in the heterogeneous photo-Fenton reactions, the concentration of $O_2^{\cdot-}$ in the $BiVO_4$/Fh system was much lower than that in the Fh system, while the concentration of $HO^{\cdot}$ exhibited the opposite trend [4]. These results showed that directly injecting photo-generated electrons from $BiVO_4$ to Fh can inhibit the reaction between Fe(III) and H_2O_2, thus restraining the generation of $O_2^{\cdot-}$. However, in this work, the $O_2^{\cdot-}$ in the CNTs/Fh system also plays an important role in the degradation of BPA, further indicated that CNTs can promote the reduction of Fe(III) by H_2O_2, along with the increased generation of $O_2^{\cdot-}$.

Furthermore, the concentrations of $HO^{\cdot}$ in the heterogeneous Fenton reaction were measured using BA as an $HO^{\cdot}$ probe (Fig. 4f). The $HO^{\cdot}$ concentration is rather low in the pure CNTs system, in agreement with the rather weak decomposition of H_2O_2 (Fig. 3e). The $HO^{\cdot}$ concentration is about 15.1 μmol/L within 60 min in the pure Fh system, and the introduction of CNTs can significantly enhance the production of $HO^{\cdot}$ concentration in the CNTs/Fh systems. Noticeably, the $HO^{\cdot}$ concentration of 3%CNTs/Fh can reach 26.4 μmol/L within 60 min, which is much higher than that of pure Fh. The concentrations of the produced $HO^{\cdot}$ in these Fenton reaction systems are well consistent with the H_2O_2 decomposition efficiency (Fig. 3e), the Fe(II) generation efficiency (Fig. 4a), and the heterogeneous Fenton catalytic activities (Fig. 3a).

3.5. DFT calculations and CV analysis of the catalysts

The DFT-optimized structures of Fh, CNTs (with a single COOH

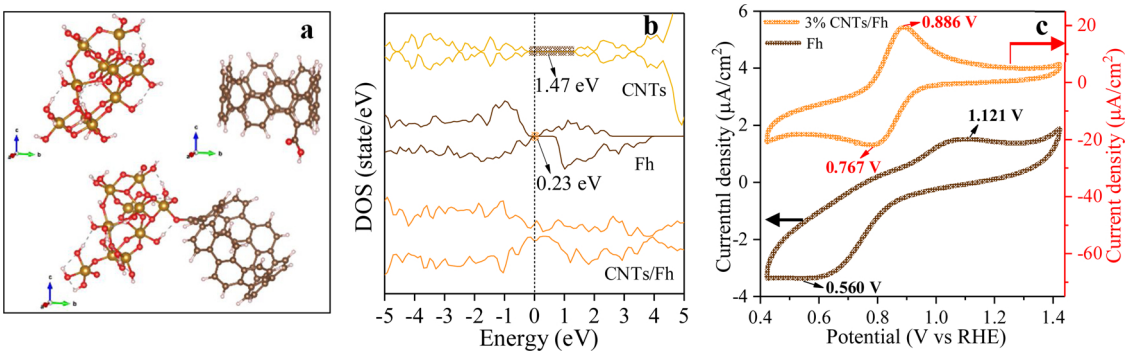

Fig. 5. (a) DFT-optimized structure of Fh, CNTs with a single COOH substituent at the rim, and CNTs/Fh (The CNTs substrate is an infinitely extended structure. The connection between CNTs and Fh in the illustration does not represent the edge modification); (b) Density of states (DOS) of Fh, CNTs, and CNTs/Fh composites; (c) Cyclic voltammograms of Fh and 3%CNTs/Fh at scan rate of 10 mV/s in 0.5 M Na_2SO_4 solution (pH = 3).

substituent at the rim), and CNTs/Fh were presented in Fig. 5a. Fh and CNTs are connected via Fe—O—C bonds (Fig. S6). The highest occupied molecular orbital (HOMO), the lowest unoccupied molecular orbital (LUMO), and the HOMO-LUMO gap were calculated to study the chemical reactivity of the as-prepared catalysts. The HOMO-LUMO gap of CNTs is 1.47 eV (Fig. 5b and Table S3), well consistent with the results of the previous studies, i.e., the HOMO-LUMO gap of functionalized CNTs was about 1.33–1.70 eV [59,60]; while the HOMO-LUMO gap of Fh is 0.23 eV. After combing CNTs with Fh, the HOMO-LUMO gap of CNTs/Fh disappeared, indicating the presence of electrons at the Fermi energy of CNTs/Fh. In particular, the density of states for different elements of CNTs/Fh shows that the electrons at the Fermi energy of CNTs/Fh are mainly from the d, p, and p orbits of Fe, O, and C atoms, respectively. These results indicated that these electrons at the Fermi energy of CNTs/Fh both from CNTs and Fh, suggesting the strong electron-electron interaction in the CNTs/Fh composites. Lyu et al. studied the electronic properties of 4-phenoxyphenol-functionalized reduced graphene oxide nanosheets (POP-rGO NSs) via DFT calculations [61]. They found that the HOMO–LUMO gap of POP-rGO NSs decreased as compared to POP and graphene, proposing that the electron transfer was accelerated between POP and rGO. Accordingly, they suggested that the chemical reactivity of POP-rGO NSs could be significantly higher than that of graphene and POP. Similarly, in our study, the disappeared HOMO–LUMO gap for CNTs/Fh also reveals that the electron transfer in CNTs/Fh should be accelerated, which will dynamically enhance the electron exchange between H_2O_2 and Fh, resulting in the promoted decomposition of H_2O_2, well cosistent with above experimental results (i.e., the promoted decomposition of H_2O_2, accelerated regeneration of Fe(II), and enhanced production of $HO^{\cdot}$).

The CV curves were measured to investigate the redox potential of Fh and 3%CNTs/Fh (Fig. 5c). Two very weak peaks (an oxidation peak at 1.1 V vs RHE and a reduction peak at 0.56 V vs RHE) appeared in the CV of Fh modified electrode (Fig. 5c and S7), indicating the presence of weak Fe(III)/Fe(II) redox reactions in Fh. The quasi-reversible CV curve of 3%CNTs/Fh exhibits two strong peaks located at 0.767 and 0.886 V vs RHE. The current intensity of these two peaks, especially for the reduction peak, enhances obviously in the CV curve of 3%CNTs/Fh (i.e., increasing from -3.35 to -21.8 μA/cm^3 for the reduction peak and from 1.52 to 19.4 μA/cm^3 for the oxidation peak, respectively), suggesting that the Fe(III)/Fe(II) redox cycling in 3%CNTs/Fh is significantly accelerated with the introduction of CNTs, well in agreement with above DFT calculation results. These results together proved that the reaction between CNTs/Fh and H_2O_2 can be dynamically accelerated.

Moreover, the half-wave potential ($E_{1/2}$) (i.e., [$E_{(\text{reduction potential})} + E_{(\text{oxidation potential})}$]/2) of CNTs/Fh is about 0.827 V vs. RHE, which is lower than that of Fh (0.841 V vs. RHE) (Table S4), indicating that the accelerated reduction of Fe(III) in the CNTs/Fh system. Similar results were obtained by Huang et al. [62]. They demonstrated that the $E_{1/2}$ of Fe(III)/Fe(II)–EDDS complex was 0.069 V/NHE, which was slightly lower (29 mV) than the $E_{1/2}$ obtained under the same pH condition for the Fe(III)/Fe(II)–EDTA complex (0.098 V/NHE), resulting in higher photo-Fenton efficiency for Fe(III)-EDDS. These results verified our hypothesis that CNTs with abundant oxygen-containing functional groups could be complexed with Fh (formed Fe—O—C bonds) to lower the redox potential of Fe(III)/Fe(II). As a result, the reduction of Fe(III) to Fe(II) will be thermodynamically more favorable for CNTs/Fh than for Fh.

Another apparent difference in the CV curve between Fh and 3%CNTs/Fh is their $\triangle E$ value (i.e., $E_{(\text{oxidation potential})}$-$E_{(\text{reduction potential})}$). The $\triangle E$ value for Fe(III)/Fe(II) redox of 3%CNTs/Fh (0.12 V vs RHE) is much lower than that of Fh (0.56 V vs RHE) (Table S4), which indicated that the reversibility of Fe(III)/Fe(II) redox in 3%CNTs/Fh was enhanced, and thus the structural stability of CNTs/Fh composites could be enhanced. These results were well consistent with the results of repeatability experiments, which showed that the degradation of BPA by 3%CNTs/Fh can retain 99.6 % after 4 cycles (Fig. 3c). A similar phenomenon could also be observed in the CV curves of Fe amidoximated polyacrylonitrile (Fe-AO-PAN) and Cu–Fe-AO-PAN (II) in other literature [63]. The $\triangle E$ value for Fe(III)/Fe(II) redox of Cu–Fe-AO-PAN (II) was much lower than that of Fe-AO-PAN, which was attributed to the rapid transformation of Fe(III)/Fe(II) in Cu–Fe-AO-PAN (II). The above results revealed that the structural stability of CNTs/Fh was enhanced, suggesting that CNTs/Fh could serve as highly-effective and stable heterogeneous Fenton catalysts.

In conclusion, these CV results demonstrated that the introduction of CNTs could enhance the Fe(III)/Fe(II) redox cycling of CNTs/Fh during Fenton reaction, from both dynamic (accelerating the electron transfer from H_2O_2 to Fh) and thermodynamic (lowering the redox potential of Fe(III)/Fe(II)) aspects, which subsequently could well promote the decomposition of H_2O_2 and the production of $HO^{\cdot}$, making CNTs/Fh composites highly effective heterogeneous Fenton catalysts. In addition, combing CNTs with Fh could also enhance the structural stability of Fh, resulting in the high Fenton activity of CNTs/Fh after being reused for four cycles.

3.6. Heterogeneous Fenton catalytic mechanisms

A number of strategies have been developed in previous studies to improve the heterogeneous Fenton catalytic efficiency [3–5,15,34,64,65]. For example, the UV–vis light irradiation (i.e., photolysis of Fe-OH) and the direct electron injection of external electrons (from electron-rich materials, semiconductor, or plasmonic materials) could all accelerate the reduction of Fe(III) to Fe(II) [3–5]; and the complexation of Fe(III)/Fe(II) with carboxylates (e.g., EDTA and oxalate) might decrease the Fe(III)/Fe(II) redox potential [15,34]. These methods, from dynamic and/or thermodynamic aspects, can promote the decomposition rate of H_2O_2 and generation of $HO^{\cdot}$, leading to enhanced heterogeneous Fenton reactivity.

In this work, we propose that the significant enhancement of Fenton reactivity for CNTs/Fh (as compared with Fh) should arise from both dynamic and thermodynamic aspects (Scheme 1). As discussed above, the DFT calculation results indicated that the electron conductivity for CNTs/Fh composites was enhanced, which could dynamically accelerate the electron transfer between the composites and H_2O_2. The enhanced conductivity was further proved by the CV results, which demonstrated that the intensity of the oxidation and reduction peaks for CNTs/Fh was much stronger than that of Fh. On the other hand, the CV results further showed that the redox potential of Fe(III)/Fe(II) could be thermodynamically lowered for the CNTs/Fh composites. These results well showed that the Fe(III)/Fe(II) redox cycling on CNTs/Fh could be significantly enhanced from both dynamic and thermodynamic point of view, which subsequently can well promote the decomposition of H_2O_2 and the production of $HO^{\cdot}$, making CNTs/Fh composites highly effective heterogeneous Fenton catalysts. Moreover, our results from Fenton catalytic reaction and CV characterization showed that the structural stability of CNTs/Fh composites could be well retained during the Fenton reaction process, which further added the applicability of these CNTs/Fh composites in environmental remediations.

4. Conclusion

In this work, for the first time, we successfully synthesized highly effective heterogeneous Fenton catalysts (i.e., CNTs/Fh), by simply combining CNTs with Fh via a facile stirring method. The BPA degradation rates of CNTs/Fh increased dramatically and the K_{app} by 3%CNTs/Fh could even reach ~7.1 times as high as that by pure Fh. In addition, CNTs/Fh could maintain high Fenton activity after being reused for four cycles, and the XPS results showed that the graphitic structure of used CNTs is quite stable. Combining the experimental results (i.e., H_2O_2 decomposition, Fe(II) regeneration, and $HO^{\cdot}$ production), CV characterization, and DFT calculations, the possible

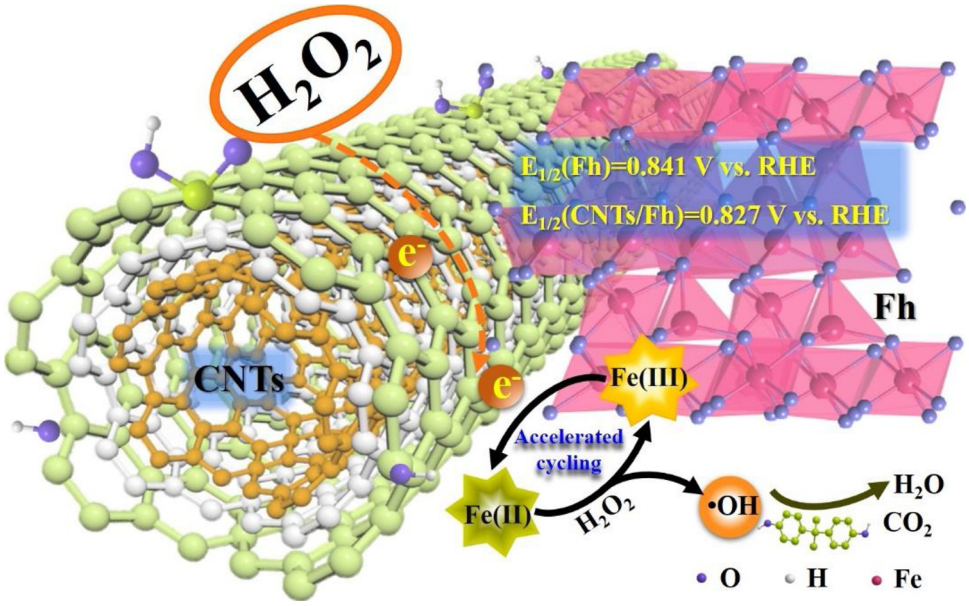

Scheme 1. Possible heterogeneous Fenton catalytic mechanism in the CNTs/Fh system.

mechanisms for the enhanced Fenton reactivity of CNTs/Fh were deduced. After the introduction of CNTs, the Fe(III)/Fe(II) redox cycling on CNTs/Fh could be significantly enhanced during Fenton reaction, from both dynamic (accelerating the electron transfer from H_2O_2 to Fh) and thermodynamic (lowering Fe(III)/Fe(II) redox potential) aspects, resulting in the enhancement of the decomposition of H_2O_2 and the production of HO˙. This study suggested that the carbon materials-iron (hydr)oxides composites may serve as promising materials due to the excellent conductivity of carbon materials and the complexation reaction between functionalized carbon materials and iron (hydr)oxides, and these composites should have potential applications in both wastewater treatment and soil remediation.

CRediT authorship contribution statement

Runliang Zhu: Conceptualization, Validation, Investigation, Resources, Visualization, Writing - review & editing, Supervision, Funding acquisition. **Yanping Zhu:** Methodology, Investigation, Formal analysis, Writing - original draft. **Haiyang Xian:** Formal analysis. **Lixia Yan:** Methodology. **Haoyang Fu:** Methodology. **Gangqiang Zhu:** Supervision, Validation. **Yunfei Xi:** Writing - review & editing. **Jianxi Zhu:** Supervision. **Hongping He:** Project administration.

Declaration of Competing Interest

The authors declare that they have no known competing financial interests or personal relationships that could have appeared to influence the work reported in this paper.

Acknowledgments

This work was financially supported by the National Natural Science Foundation of China (41872044), Newton Advanced Fellowship (NA150190), National Program for Support of Top-notch Young Professionals, and China scholarship council.

Appendix A. Supplementary data

Supplementary material related to this article can be found, in the online version, at doi:https://doi.org/10.1016/j.apcatb.2020.118891.

References

[1] A.K. Patra, S.K. Kundu, A. Bhaumik, D. Kim, Nanoscale 8 (2016) 365–377.
[2] L. Wang, M. Cao, Z. Ai, L. Zhang, Environ. Sci. Technol. 48 (2014) 3354–3362.
[3] X. Hou, X. Huang, F. Jia, Z. Ai, J. Zhao, L. Zhang, Environ. Sci. Technol. 51 (2017) 5118–5126.
[4] T. Xu, R. Zhu, G. Zhu, J. Zhu, X. Liang, Y. Zhu, H. He, Appl. Catal. B 212 (2017) 50–58.
[5] X. Zhang, Y. Chen, N. Zhao, H. Liu, Y. Wei, RSC Adv. 4 (2014) 21575–21583.
[6] M. Munoz, Z.M. de Pedro, J.A. Casas, J.J. Rodriguez, Appl. Catal. B 176–177 (2015) 249–265.
[7] N.A. Zubir, C. Yacou, J. Motuzas, X. Zhang, X.S. Zhao, J.C. Diniz da Costa, Chem. Commun. 51 (2015) 9291–9293.
[8] Y. Zhu, R. Zhu, L. Yan, H. Fu, Y. Xi, H. Zhou, G. Zhu, J. Zhu, H. He, Appl. Catal. B 239 (2018) 280–289.
[9] Y. Zhu, R. Zhu, Y. Xi, T. Xu, L. Yan, J. Zhu, G. Zhu, H. He, Chem. Eng. J. 346 (2018) 567–577.
[10] J. Shi, Z. Ai, L. Zhang, Water Res. 59 (2014) 145–153.
[11] W. Shi, D. Du, B. Shen, C. Cui, L. Lu, L. Wang, J. Zhang, ACS Appl. Mater. Interfaces 8 (2016) 20831–20838.
[12] Z. Ai, Z. Gao, L. Zhang, W. He, J.J. Yin, Environ. Sci. Technol. 47 (2013) 5344–5352.
[13] H. Wu, Z. Ai, L. Zhang, Water Res. 52 (2014) 92–100.
[14] X. Huang, X. Hou, F. Song, J. Zhao, L. Zhang, J. Phys. Chem. C 121 (2017) 1113–1121.
[15] N. Wang, L. Zhu, M. Lei, Y. She, M. Cao, H. Tang, ACS Catal. 1 (2011) 1193–1202.
[16] T. Xu, R. Zhu, H. Shang, Y. Xia, X. Liu, L. Zhang, Water Res. 159 (2019) 10–19.
[17] Y. Ding, W. Huang, Z. Ding, G. Nie, H. Tang, Sep. Purif. Technol. 168 (2016) 223–231.
[18] A. Babuponnusami, K. Muthukumar, J. Environ. Chem. Eng. 2 (2014) 557–572.
[19] Y. Deng, M. Xing, J. Zhang, Appl. Catal. B: Environ. 211 (2017) 157–166.
[20] Y. Hou, Y. Wang, H. Yuan, H. Chen, G. Chen, J. Shen, L. Li, J. Nanoparticle Res. 18 (2016).
[21] Y. Yao, H. Chen, J. Qin, G. Wu, C. Lian, J. Zhang, S. Wang, Water Res. 101 (2016) 281–291.
[22] Z. Yang, A. Yu, C. Shan, G. Gao, B. Pan, Water Res. 137 (2018) 37–46.
[23] M. Feng, R. Qu, X. Zhang, P. Sun, Y. Sui, L. Wang, Z. Wang, Water Res. 85 (2015) 1–10.
[24] T. Xu, R. Zhu, J. Liu, Q. Zhou, J. Zhu, X. Liang, Y. Xi, H. He, J. Mol. Catal. A Chem. 424 (2016) 393–401.
[25] L. Yu, J. Chen, Z. Liang, W. Xu, L. Chen, D. Ye, Sep. Purif. Technol. 171 (2016) 80–87.
[26] F. Lücking, H. Köser, M. Jank, A. Ritter, Water Res. 32 (1998) 2607–2614.
[27] T.A. Kurniawan, W.H. Lo, Water Res. 43 (2009) 4079–4091.
[28] G. Fang, C. Liu, J. Gao, D.D. Dionysiou, D. Zhou, Environ. Sci. Technol. 49 (2015) 5645–5653.
[29] G. Fang, J. Gao, C. Liu, D.D. Dionysiou, Y. Wang, D. Zhou, Environ. Sci. Technol. 48 (2014) 1902–1910.
[30] Y. Qin, L. Zhang, T. An, ACS Appl. Mater. Interfaces 9 (2017) 17115–17124.
[31] J. Ma, M. Yang, F. Yu, J. Chen, J. Colloid Interface Sci. 444 (2015) 24–32.
[32] J. Seo, H.-J. Lee, H. Lee, H.-E. Kim, J.-Y. Lee, H.S. Kim, C. Lee, Chem. Eng. J. 273 (2015) 502–508.
[33] J. Peng, J. Xue, J. Li, Z. Du, Z. Wang, S. Gao, Chem. Eng. J. 321 (2017) 325–334.
[34] T.J. Strathmann, A.T. Stone, Environ. Sci. Technol. 36 (2002) 5172–5183.

[35] M.F. Hochella Jr., D.W. Mogk, J. Ranville, I.C. Allen, G.W. Luther, L.C. Marr, B.P. McGrail, M. Murayama, N.P. Qafoku, K.M. Rosso, N. Sahai, P.A. Schroeder, P. Vikesland, P. Westerhoff, Y. Yang, Science 363 (2019).
[36] H. Fu, Y. Yang, R. Zhu, J. Liu, M. Usman, Q. Chen, H. He, J. Colloid Interface Sci. 530 (2018) 704–713.
[37] J.C. Barreiro, M.D. Capelato, L. Martin-Neto, H.C. Bruun Hansen, Water Res. 41 (2007) 55–62.
[38] G. Kresse, J. Furthmüller, Comput. Mater. Sci. 6 (1996) 15–50.
[39] G. Kresse, D. Joubert, Phys. Rev. B 59 (1999) 1758–1775.
[40] J.A. Halfen, S. Mahapatra, E.C. Wilkinson, S. Kaderli, V.G. Young, L. Que, A.D. Zuberbühler, W.B. Tolman, Science 271 (1996) 1397.
[41] Z. Yin, Phys. Rev. B 82 (2010) 155202.
[42] F.M. Michel, L. Ehm, S.M. Antao, P.L. Lee, P.J. Chupas, G. Liu, D.R. Strongin, M.A. Schoonen, B.L. Phillips, J.B. Parise, Science 316 (2007) 1726–1729.
[43] V.F. Samanidou, M.A. Frysali, I.N. Papadoyannis, J. Liq, Chromatogr. Relat. Technol. 37 (2014) 247–258.
[44] K. Kosaka, H. Yamada, S. Matsui, S. Echigo, K. Shishida, Environ. Sci. Technol. 32 (1998) 3821–3824.
[45] S.H. Joo, A.J. Feitz, D.L. Sedlak, T.D. Waite, Environ. Sci. Technol. 39 (2005) 1263–1268.
[46] C.R. Keenan, D.L. Sedlak, Environ. Sci. Technol. 42 (2008) 1262–1267.
[47] G. Ovejero, J. Sotelo, M. Romero, A. Rodríguez, M. Ocana, G. Rodríguez, J. Garcia, Ind. Eng. Chem. Res. 45 (2006) 2206–2212.
[48] Y. Lee, W. Lee, J. Hazard. Mater. 178 (2010) 187–193.
[49] B.-S. Zhu, Y. Jia, Z. Jin, B. Sun, T. Luo, L.-T. Kong, J.-H. Liu, RSC Adv. 5 (2015) 84389–84397.
[50] R. Arrigo, M. Hävecker, S. Wrabetz, R. Blume, M. Lerch, J. McGregor, E.P. Parrott, J.A. Zeitler, L.F. Gladden, A. Knop-Gericke, J. Am. Chem. Soc. 132 (2010) 9616–9630.
[51] X. Yan, X. Xu, Q. Liu, J. Guo, L. Kang, J. Yao, J. Power Sources 389 (2018) 260–266.
[52] A.G. Nene, M. Takahashi, P.R. Somani, H. Aryal, K. Wakita, M. Umeno, Carbon: Sci.Technol. 8 (2016) 13–24.
[53] C. Fu, G. Zhao, H. Zhang, S. Li, Int. J. Electrochem. Sci. 9 (2014) 46–90.
[54] D.N. Futaba, K. Hata, T. Yamada, T. Hiraoka, Y. Hayamizu, Y. Kakudate, O. Tanaike, H. Hatori, M. Yumura, S. Iijima, Nat. Mater. 5 (2006) 987–994.
[55] S.A.C. Carabineiro, T. Thavorn-amornsri, M.F.R. Pereira, P. Serp, J.L. Figueiredo, Catal. Today 186 (2012) 29–34.
[56] W.-J. Yu, P.-X. Hou, F. Li, C. Liu, J. Mater. Chem. 22 (2012) 13756.
[57] C. Annese, L. D'Accolti, G. Giambastiani, A. Mangone, A. Milella, G. Tuci, C. Fusco, Eur. J. Org. Chem. 2014 (2014) 1666–1671.
[58] X. Hu, B. Liu, Y. Deng, H. Chen, S. Luo, C. Sun, P. Yang, S. Yang, Appl. Catal. B: Environ. 107 (2011) 274–283.
[59] H. Soleymanabadi, J. Kakemam, Physica E 54 (2013) 115–117.
[60] R. Khorrampour, M.D. Esrafili, N.L. Hadipour, Physica E 41 (2009) 1373–1378.
[61] L. Lyu, G. Yu, L. Zhang, C. Hu, Y. Sun, Environ. Sci. Technol. 52 (2018) 747–756.
[62] W. Huang, M. Brigante, F. Wu, C. Mousty, K. Hanna, G. Mailhot, Environ. Sci. Technol. 47 (2013) 1952–1959.
[63] Z. Han, Y. Dong, S. Dong, J. Hazard. Mater. 189 (2011) 241–248.
[64] N. Mishra, R. Reddy, A. Kuila, A. Rani, A. Nawaz, S. Pichiah, Curr. World Environ. 12 (2017) 469–489.
[65] S. Rahim Pouran, A.A. Abdul Raman, W.M.A. Wan Daud, J. Clean. Prod. 64 (2014) 24–35.